Solid State Ionics 225 (2012) 176–181

Contents lists available at SciVerse ScienceDirect

Solid State Ionics

journal homepage: www.elsevier.com/locate/ssi

A combinatorial nanoprecursor route for direct solid state chemistry: Discovery and electronic properties of new iron-doped lanthanum nickelates up to $La_4Ni_2FeO_{10-\delta}$

Sam J. Alexander [a], Tian Lin [d], Dan J.L. Brett [b], Julian R.G. Evans [a], Giannantonio Cibin [c], Andrew Dent [c], Gopinathan Sankar [a], Jawwad A. Darr [a,*]

[a] Department of Chemistry, University College London, 20 Gordon Street, London, WC1H OAJ, United Kingdom
[b] Department of Chemical Engineering, University College London, Torrington Place, WC1E 6BT, United Kingdom
[c] Diamond Light Source, Harwell Science and Innovation Campus, Didcot, Oxfordshire, OX11 0DE, United Kingdom
[d] Institute for Particle Science and Engineering, School of Process, Environmental and Materials Engineering, University of Leeds, Houldsworth Building, Clarendon Road, Leeds, LS2 9JT, United Kingdom

ARTICLE INFO

Article history:
Received 1 September 2011
Received in revised form 10 April 2012
Accepted 25 April 2012
Available online 1 June 2012

Keywords:
Continuous hydrothermal flow synthesis
Combinatorial
High-throughput
Ruddlesden Popper

ABSTRACT

We describe a simple nanoprecursor route for direct solid-state combinatorial synthesis and discovery of heterometallic materials compositions which are normally difficult to make in a single step. Using a combinatorial robot (incorporating a continuous hydrothermal reactor), co-precipitated nanoprecursors containing different amounts of La, Ni and Fe oxides were made. These samples were divided into two identical cloned libraries, which were heat-treated to bring about solid-state transformations at either 1348 K or 1573 K for 12 h. In each case, experimental conditions were designed to form the corresponding $La_4Ni_{3-x}Fe_xO_{10}$ phases ($x = 0.0–3.0$) directly without comminution. Such materials are difficult to make without multiple heating and grinding steps. The heat-treated samples from each library were embedded into a wellplate and analysed by powder X-ray diffraction methods in order to elucidate trends in phase behaviour. Several hitherto unknown phase-pure Ruddlesden Popper type $La_4Ni_{3-x}Fe_xO_{10}$ compositions were identified and their DC electrical conductivities measured.

1. Introduction

Combinatorial methods in solid-state chemistry have lagged far behind those used in organic synthesis. From the mid 1990's onwards, thin film techniques were used for combinatorial searches of new inorganic superconductors [1] and phosphors [2]. However, it was often difficult subsequently to make large amounts of such materials in a reproducible way for confirmatory testing. In order to accelerate the pace of inorganic materials discovery, high-throughput automated synthesis methods were devised, where robots were used to take up much of the laborious work and also to provide consistency and accuracy [3–5]. These robots were largely involved in mixing of pre-prepared slurries or metal salt solutions. In the quest for new inorganic technological materials, observed properties are greatly influenced by the actual method of synthesis of the compound. Sometimes anomalous property measurements can arise as a consequence of an uneven distribution of metal ions in a ceramic material as a direct result of the synthesis route. Robotic printing systems for inorganic suspensions (or solutions) have been reported frequently in the literature [3,6,4,7]. LUSI (London University Search Instrument) is one such system, which is designed to ink-jet print ceramic suspensions and sinter them in a multi-zone furnace at up to 1872 K [8–10]. Parkinson and co-workers, used automation to meter and mix metal salt solutions, allowing initial homogenous mixtures of metal ions to be made that were subsequently heat-treated. This produced new photoelectrolysis catalysts; the rate limiting step in identification of active catalysts then being the screening step [11]. Combinatorial approaches to sol–gel [12], combustion [13], pulsed laser ablation [14], batch hydrothermal [15], and sputtering methods [16], are also known.

Continuous hydrothermal flow synthesis (CHFS) reactors have been used extensively by the authors previously to rapidly and efficiently produce inorganic metal oxide nanoparticles from pre-mixed metal salt solutions which can be co-precipitated as homogeneously mixed oxides or solid solutions. The CHFS process involves the reaction of a flowing solution of metal salts that is mixed with a flow of supercritical water at 450 °C and 24.8 MPa resulting in rapid nanoparticle nucleation and crystallisation [17–23]. More recently, the authors reported a development of a manual high-throughput continuous hydrothermal (HiTCH) flow synthesis reactor which can produce many compositionally unique metal oxide nanomaterials in a matter of hours, allowing greater throughput (but smaller sample size) compared to CHFS. The manual HiTCH reactor was used to produce an entire 66 sample library of $Ce_xZr_YY_zO_2$ in *ca.* 12 h [24]. Samples then had to be manually cleaned, printed and heat-treated, which was labour intensive. In a recent report

* Corresponding author. Tel.: +44 2076794345.
E-mail address: j.a.darr@ucl.ac.uk (J.A. Darr).

0167-2738/$ – see front matter © 2012 Elsevier B.V. All rights reserved.
doi:10.1016/j.ssi.2012.04.027

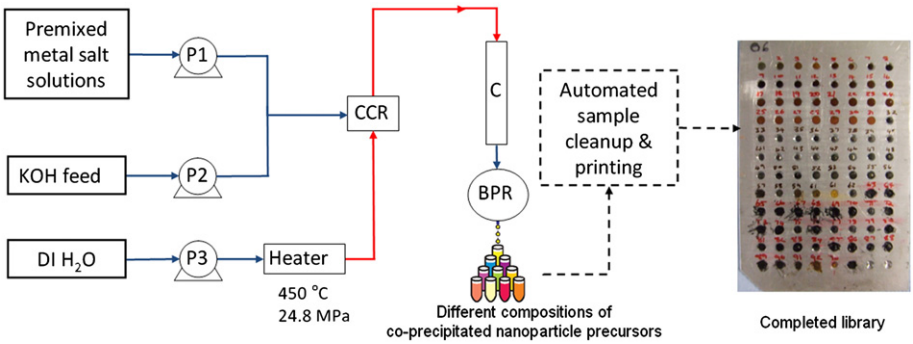

Fig. 1. Scheme of HiTCH, P = pump, CCR = co-current reactor, C = cooler, BPR = back pressure regulator.

by the authors, a combinatorial synthesis robot, RAMSI (rapid automated materials synthesis instrument) was developed [25]. RAMSI is a fully automated materials synthesis platform that can rapidly produce nanopowders which in turn can act as precursors for solid-state reactions in order to discover new materials. In RAMSI, metal salts are automatically mixed and introduced into an automated HiTCH flow synthesis system and collected as nanoparticle slurries at the outlet of the reactor after cooling in-line, as shown in Fig. 1. Thereafter, sample clean-up and printing of samples as dried ceramic dots is carried out using a robot arm and carousels containing various liquid handling functions in RAMSI.

Herein we describe the use of RAMSI to synthesise the full range of metal hydroxide nanoprecursors for the system $La_4Ni_{3-x}Fe_xO_{10}$ (where $x = 0.0–3.0$ and $\Delta x = 0.1$). The set of nanoprecursors were printed as ceramic dots, which when dried were split into two cloned libraries. The cloned libraries were then heat-treated at different temperatures to bring about solid-state reactions. The DC electrical conductivities of the resulting phase pure materials were then tested.

2. Experimental details

2.1. Syntheses of nanopowder precursor co-precipitates via RAMSI

The source materials [$La(NO_3)_3 \cdot 6H_2O$] (99.9%), [$Ni(NO_3)_2 \cdot 6H_2O$] (99.9%) and [$Fe(NO_3)_3 \cdot 9H_2O$] (99.9%) were supplied by Sigma-Aldrich Chemical Company (Dorset, UK). KOH pellets (≥85%) were supplied by Fisher Scientific Chemical Company (Loughborough, UK). All experiments were conducted using deionised water (10 MΩ) throughout.

A set of co-precipitated nanoprecursors were synthesised using the synthesis module within RAMSI. This was essentially a fully automated high throughput continuous hydrothermal (HiTCH) flow synthesis reactor, details of which have been reported elsewhere including the synthesis hardware and functions of RAMSI [25]. The order of both synthesis and cleanup actions are presented in the Supplementary data. The synthesis was as follows; 1.0 L (0.1 M) metal salt stock solutions were made by accurately weighing $La(NO_3)_3 \cdot 6H_2O$ (43.30 g) and deionised water added to a final volume of 1.0 L. The same procedure was carried out for $Ni(NO_3)_2 \cdot 6H_2O$ (29.10 g) and $Fe(NO_3)_3 \cdot 9H_2O$ (40.40 g). Thereafter, the desired molar ratios of the 31 compositions for the co-precipitates corresponding to $La_4Ni_{3-x}Fe_xO_{10}$ (where $x = 0.0–3.0$ and $\Delta x = 0.1$) were entered into the RAMSI GUI interface.

In the automated HiTCH process described above, each metal salt composition (25 mL) was introduced into the hydrothermal apparatus, where it was mixed with 1 mol KOH solution to attain a basic pH at a T-piece mixer. Pump rates were set to 20 mL min^{-1} pump 1 (P1) and 10 mL min^{-1} for pumps 2 and 3 (P2, P3) as shown in Fig. 1. Each sample then met a stream of supercritical water (sc-H_2O) (which was at 450 °C, 24.8 MPa) in a co-current mixer (made of Swagelok™ stainless steel fittings) (GB patent pending 335328) whereupon rapid hydrolysis and subsequent dehydration occurred (in seconds) to produce nanosized metal oxide co-precipitates. After synthesis, the nanoparticles passed through a vertical water-cooled pipe and then exited the system through the backpressure regulator where they were collected as a slurry.

The nanopowder co-precipitate slurries were collected on the RAMSI collection carousel and produced a total of 31 filled falcon tubes (one 50 mL tube for each composition) which were collected

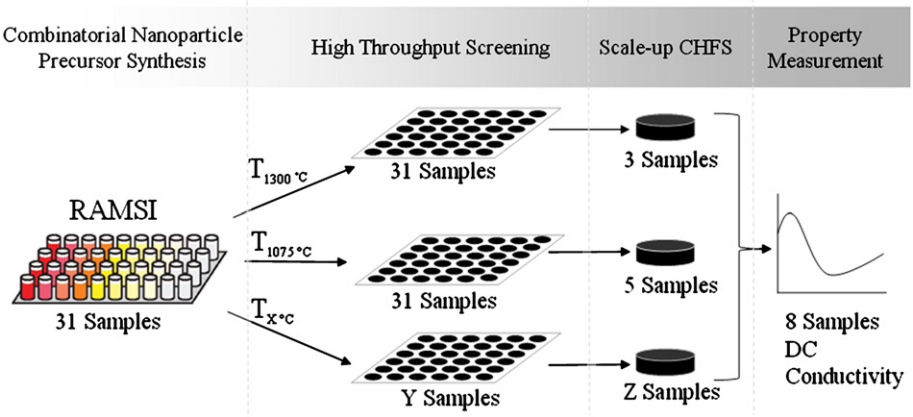

Fig. 2. Schematic representation of the combinatorial synthesis and screening strategy.

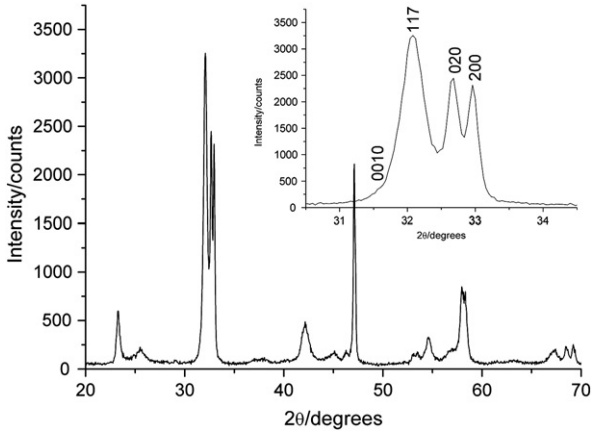

Fig. 3. X-ray diffraction pattern of $La_4Ni_{2.7}Fe_{0.3}O_{10}$. Inset: expanded peak highlighting the strong anisotropic broadening in the c direction.

in sequence and then placed into a tube rack by the robot arm to be later cleaned up and printed as dots (more than one tube per sample can be made if required).

2.2. Analytical measurements

Powder X-ray diffraction (PXRD) was conducted using a Bruker-AXS D8 (GADDS) diffractometer. This instrument used a large 2D area detector to record large sections of multiple Debye–Scherrer cones simultaneously. Both θ and ω could be measured with 0.01° resolution using a Cu ($K\alpha_1$ and $K\alpha_2$) radiation source. After collection, the data across the Debye–Scherrer cones could be integrated across ω to produce a standard one-dimensional, 2θ against intensity plot. This diffractometer was equipped with a programmable table allowing the collection of up to 66 patterns, in-line in one night. PXRD data for closer analysis (around phase boundaries) were collected on a flatplate Bruker D4 diffractometer using Cu ($K\alpha_1$ and $K\alpha_2$) radiation. Data were collected over the 2θ range 20–70° with a step size of 0.05° and a count time of 4 s per step. Unit cell sizes were determined using the Celref program based on Bmab and Fmmm space groups. Room temperature Fe K-edge EXAFS data were collected at B18 beam line at Diamond Light Source which operates at 3 GeV with a typical beam current of *ca.* 200 mA [26]. This beam line is equipped with Si(111) double-crystal monochromator and ion-chambers for measuring incident and transmitted beam intensity. In addition, a 9 element Ge Canberra detector is also available for measurements in fluorescence mode; all the data were collected in fluorescence mode. The data were processed using VIPER and EXCURVE software. Raw data were analysed without Fourier filtering and a multiple-scattering method was employed to obtain the best fit taking into account near-neighbour distances of *ca.* 4.5 Å.

Phase-pure samples were prepared as round pellets typically ø = 13 mm and thickness = 1 mm which were sintered in air at 1473 K for 12 h.

The electronic conductivity of the samples was measured using the four-probe Van der Pauw technique [27]. A thermocouple was placed in close proximity to the sample. Four platinum contacts (1, 2, 3, and 4) were positioned symmetrically in a square arrangement at the periphery of one face of the sample discs. The potential drop between 1 and 2, 2 and 3, 3 and 4, and 4 and 1 was measured using a PeakTech 4000 Digital multimeter while applying a certain DC bias to maintain a current of 0.5 Å, using a PeakTech 6036D DC multi-output power supply, through the opposing pairs of contacts.

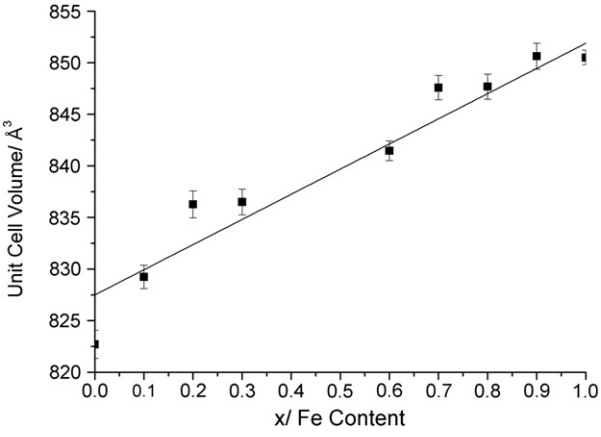

Fig. 4. Unit cell volume as a function of iron content for the $La_4Ni_{3-x}Fe_xO_{10}$ series.

3. Results and discussion

The synthesis strategy (which is outlined in Fig. 2) was the automated synthesis of 31 nanoprecursor slurries for the system $La_4Ni_{3-x}Fe_xO_{10}$ (x = 0.0–3.0, Δx = 0.1) which could then be placed into cloned libraries, and heat-treated at two different temperatures to bring about solid-state transformations. 31 dark slurries (that became browner with increasing Fe content) were made using an automated HiTCH nanoparticle synthesis system, which is an integral part of RAMSI, (Fig. 1) (using supercritical water feed at 723 K and 24.8 MPa as a reagent). A throughput of 7.5 samples h^{-1} was achieved. After synthesis, the collected sample tubes were automatically grouped by RAMSI for centrifuging and supernatant replacement in sequence. The samples were obtained as thirty dark coloured slurries after automated clean-up and were placed in racks prior to printing. In order to deliver ceramic dots which would dry intact and survive after heat-treatment, a concentration of *ca.* 1.0 ± 0.2 g mL^{-1} was chosen as the optimum after trial and error, this concentration was achieved by manual addition of deionised water. When the sample dots had been dried in air, all samples were placed manually in a furnace and heat-treated at 1348 K and 1573 K for 12 h on a 2 mm thick platinum plate. The samples were then manually fixed flat side up into a custom made 96 well aluminium wellplate.

Each wellplate was analysed using automated powder XRD and these patterns quickly highlighted a possible phase boundary region for $La_4Ni_{3-x}Fe_xO_{10}$ that was *ca.* x = 0.3–0.5 (precise identification was difficult due to the quality of the data obtained from the wellplate) for the library heat-treated at 1348 K for 12 h. In contrast, XRD analysis of the cloned library heat-treated at 1573 K for 12 h, suggested that the phase boundary for $La_4Ni_{3-x}Fe_xO_{10}$ was extended as high as x = 1. In contrast, previous attempts in the literature to make phase pure $La_4Ni_{3-x}Fe_xO_{10}$ obtained an upper limit of x = 0.3 using polymerisation synthesis based methods taking 60 and 22 h, with several intermittent regrinding stages [28,29].

Once the initial X-ray screening data had been obtained, eight larger sample sizes (*ca.* 0.5 g each) were remade using a manual CHFS reactor for key compositions around the suggested phase boundaries to obtain higher resolution X-ray data and samples for DC electrical testing (Fig. 2). Unit cell parameters were calculated using the Fmmm and Bmab space groups as a model, as previously suggested [30,31]. Orthorhombic Bmab produced a better fit in all cases of single phase materials and thus, was chosen. PXRD data confirmed that for samples heat-treated at 1348 K, a nominal Fe content as high as x = 0.3 ($La_4Ni_{3-x}Fe_xO_{10}$) was confirmed, in agreement with previously reported results in which solid-state methods were used from oxide precursors [32]. Herein, compositions where x = 0.4 and 0.5 were not very crystalline and appeared to be mixed phases of $La_4Ni_{3-x}Fe_xO_{10}$ (n = 3) and $La_2Ni_{1-x}Fe_xO_4$ (n = 2).

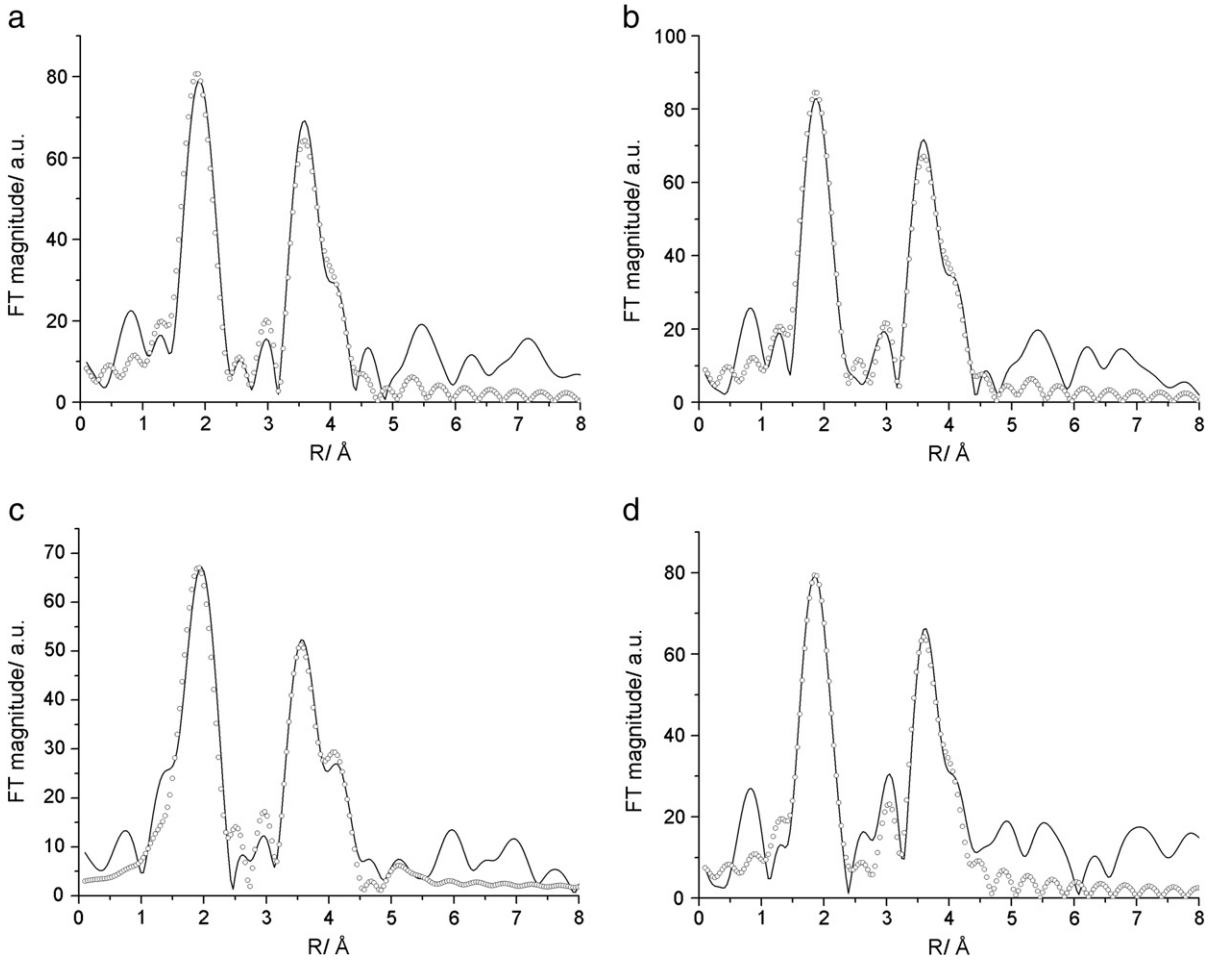

Fig. 5. EXAFS plots of a) $La_4Ni_{2.8}Fe_{0.2}O_{10}$, b) $La_4Ni_{2.7}Fe_{0.3}O_{10}$, c) $La_4Ni_{2.2}Fe_{0.8}O_{10}$ and d) $La_4Ni_{2.1}Fe_{0.9}O_{10}$. The continuous line represents the Fourier transform of experimental data and circles represent the fitted model.

Fig. 3 highlights typical data showing how at the heat-treatment temperature regime 1348 K (12 h) samples were anisotropic in the c-direction (broadened peak). This behaviour has been observed previously by Ling et al. who suggested this was due to oxygen displacement perpendicular to the perovskite layers for the $La_4Ni_3O_{10}$ structure as a result of distortion to the NiO_6 octahedra [33]. The addition of iron into the RP structure could have further increased the distortion of the octahedra and hence the observed anisotropy. For samples heat-treated at 1573 K this anisotropy was far less pronounced, the higher heat-treatment temperature for the same amount of time (12 h) had the effect of possibly annealing out some of the strain. As a result of the highly anisotropic diffraction patterns, Rietveld refinement was not possible for initial samples. However, for selected samples heat-treated at 1573 K, XRD data suggested a single phase for a Fe content up to $x = 1.0$ (i.e. up to $La_4Ni_2FeO_{10}$).

Table 1
Bond lengths and coordination numbers for selected samples in the series $La_4Ni_{3-x}Fe_xO_{10}$.

x/Fe content	Fe–O			Fe–La			Fe–Ni			R_{EXAFS}
	N	*R*	$2\sigma^2$	*N*	*R*	$2\sigma^2$	*N*	*R*	$2\sigma^2$	
0.2	6	1.944	0.019	8	3.33	0.017	6	3.82	0.028	46.69
0.3	6	1.944	0.011	8	3.34	0.017	6	3.82	0.026	43.38
0.8	6	1.960	0.017	8	3.37	0.009	6	3.86	0.027	39.28
0.9	6	1.940	0.012	8	3.34	0.015	6	3.81	0.028	54.34

Peak positions of the phases, $x = 0$–1.0 indicated that unit cell volume increased approximately linearly with increasing Fe content (Fig. 4) however it was difficult to ascertain if Vegard's law was obeyed due to the uncertainty in the unit cell volume as a result of the anisotropy in the c-direction.

Selected samples were chosen for Fe K-edge EXAFS analysis. For the analysis, we used the coordinates of $La_4Ni_3O_{10}$ reported in the ICSD crystal structure data-base [34]. Starting model was generated

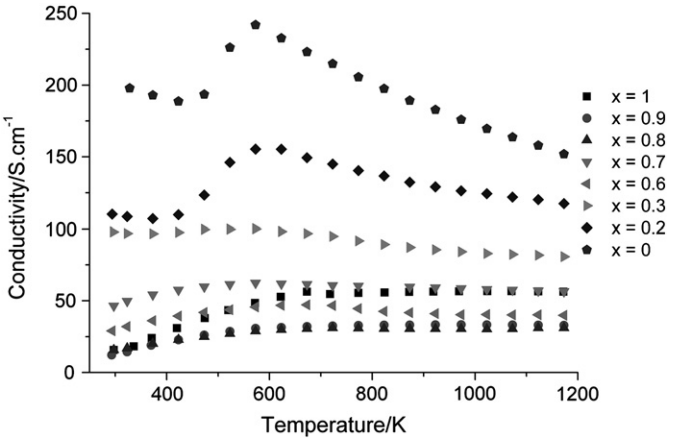

Fig. 6. Conductivity of phase pure $La_4Ni_{3-x}Fe_xO_{10}$ as a function of temperature. All samples were 59–68% of theoretical maximum density.

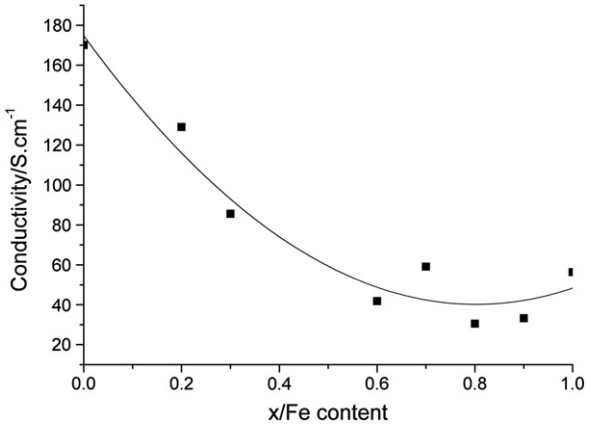

Fig. 7. Graph showing conductivity at 923 K against iron content for the $La_4Ni_{3-x}Fe_xO_{10}$ series.

in the EXCURVE program and the bond distances of various neighbours and their Debye–Waller factor were refined to obtain the best fit and they are given in Fig. 5. As mentioned earlier, a multiple-scattering method was employed here to accurately model the structure. The structural parameters obtained from the best fit are given in Table 1. Fits to the EXAFS data are supplied in the Supplementary data.

EXAFS results given in Table 1 suggested that Fe ions are located in the B (Ni) sites in all cases and did not exist as a separate iron oxide phase. In particular, all the distances obtained from the analysis using the type of near neighbour listed in the table clearly match that of the parent form $La_4Ni_3O_{10}$. An estimation of the iron oxidation state can be made using the Fe–O bond lengths that were in the range 1.944–1.960 Å, suggesting the dopant is Fe^{3+} in all cases. In the undoped $La_4Ni_3O_{10}$, charge ordering in non-equivalent NiO_6 octahedra was suggested, with preferential occupation of Ni^{3+} on the Ni1 site and Ni^{2+} on the Ni2 site [35]. Bond lengths estimating Fe^{2+} were not observed, suggesting that there is no charge ordering (i.e. no preference for Fe^{3+} on either Ni1 or Ni2 site).

Seven of the samples that were shown to be phase pure were scaled-up via a manual CHFS reactor, allowing gram-scale quantities of nanoprecursor powder to be made. Consequently, dense pressed pellets were formed by pressing powders at 6.6×10^8 Pa in a 13 mm diameter KBr die. The die was gently tapped before pressing, producing a green density in the range 53–57% of theoretical maximum density (by measurement of dimensions). By trial and error it was found that a low heating rate of 1 K min^{-1} and a sintering temperature of 1473 K for 12 h yielded pellets with sintered densities in the range 58–69% of theoretical maximum density, with no visible cracking on the surface of pellets. The densities were greater than those achieved in the comparative $La_4Ni_{3-x}Co_xO_{10}$ system by others, which were only *ca.* 40% of theoretical maximum density [30].

The conductivity as a function of temperature was measured for these discs using a standard 4-point DC probe, constructed in-house and mounted in a 7 cm diameter, 100 cm long tube furnace. The electrical conductivity of the pellets were derived using Eq. (1):

$$\sigma = \frac{\ln(2)}{\pi l} x \frac{4I}{V_{12,34} + V_{34,12} + V_{23,41} + V_{41,23}} \quad (1)$$

where σ = conductivity in S cm^{-1}, l = pellet thickness in cm, I = constant applied current in amps, and V = measured voltage in volts. The numbers in the subscripts signify the contacts through which the current was passed and the voltage measured accordingly. The resistances were calculated applying a voltage to maintain a constant current of 0.5 Å and measuring the voltage in the opposing two contacts.

Results displayed in Fig. 6 show that semiconducting behaviour was observed until ~573 K at which point metallic behaviour was generally observed for all samples. This behaviour has been observed before in the undoped analogues, and attributed to a structural phase transition from orthorhombic to tetragonal symmetry by Skinner et al. [36].

Fig. 7 displays how conductivity at 923 K generally decreased with increasing iron content to a minimum point when x = 0.8, the conductivity at 923 K, steadily decreased from 170 S cm^{-1} (density 62%) to 31 S cm^{-1} (density 58%) in the x range of 0.0–0.8, and then increased for x = 1.0 to a value of 56 S cm^{-1} (density 69%). These values compare with 50 S cm^{-1} at 923 K for $La_4Ni_{2.8}Co_{0.2}O_{10}$ (40% density) [30] and 95 S cm^{-1} at 950 K for undoped $La_4Ni_3O_{10}$ (58% density) [36]. The decreasing conductivity with increasing Fe content is most likely as a result of hole doping of the conduction band with increasing quantities of Fe(III). The small increase in conductivity when x = 1.0 that does not follow this apparent trend was caused by the increased density (~8–10% theoretical density) in comparison to the other samples. Interestingly, it was observed that at low temperatures (<773 K) upon application of a voltage to points 1 and 2 (of the 4-point DC conductivity testing apparatus where the numbering manner is clockwise and incremental from 1 to 4), the observed resistance through points 3 and 4 fell rapidly until an equilibrium value was reached. When the voltage was then removed across pins 1 and 2, the resistance measured through points 3 and 4 returned to the original value. This phenomenon was Fe dependant and the magnitude of the resistance drop increased with increasing iron dopant. The authors believe this effect could be similar to that recently reported by West and co-workers who suggested that internal electron transfer within ordered vacancy clusters in $BaTiO_3$ under a DC bias, results in a more conductive excited state that returns to the ground state when the bias is removed [37,38]. In our case, the increased doping of Fe into the La–Ni–O framework may be producing ever more charged defects into the structure, hence the magnitude of the effect is Fe dopant dependant.

4. Conclusions

In conclusion, a new approach to the "grind-free" nanoprecursor route to direct combinatorial solid state synthesis of several "difficult to make" and hitherto unknown phase-pure heterometallic Ruddlesden Popper type $La_4Ni_{3-x}Fe_xO_{10}$ materials has been described. The new approach used a high-throughput reactor and robotic automation (RAMSI) to rapidly synthesise a range of nanoparticle co-precipitate precursors in cloned libraries at a rate of 7.5 samples an hour. Each library could then be heat-treated at a different temperature and an initial powder XRD screen was used to locate and approximate phase boundary. A more focussed second synthesis and XRD characterisation of selected larger heat-treated powders was then performed to reconfirm the locations of the phase boundaries with the highest dopant level being achieved for $La_4Ni_2FeO_{10}$ which is significantly greater Fe doping than has been achieved by anyone previously (despite several notable efforts). EXAFS data suggested that Fe^{3+} was located onto Ni sites in all cases and did not exist as a separate iron oxide phase.

The DC conductivity of all the single phase materials obtained was then investigated; electronic conduction generally decreased with increasing Fe content. The combinatorial nanoprecursor route for direct solid state chemistry coupled with rapid screening has allowed the authors to make samples that were previously unknown and inaccessible via more conventional "heat and grind" or similar approaches.

Finally, the authors suggest that in the search for new doped higher order La–Ni–O RP phases, conventional solid state powder processing methods are difficult and unsuitable, whilst the nanoparticle precursor route shown herein, is highly efficient and holds great promise for accelerating future discoveries of new complex inorganic materials.

Acknowledgements

The combinatorial materials discovery robot RAMSI (Rapid Automated Materials Synthesis Instrument) was named in memory of Sir William Ramsay FRS who discovered many of the noble gasses in the late 1800s and was chair of Inorganic Chemistry at University College London (1887–1913) and a Nobel Prize winner in 1904. We thank the Engineering and Physical Research Council (EPSRC) for funding "High-Throughput Nanoceramics Discovery Project" under grant EP/D038499/1. Kathryn Thompson and Suela Kellici are acknowledged for their contributions to this project. The authors are also indebted to Labman Automation, Stokesley, UK, for the design, construction and testing and subsequent reassembly on-site of RAMSI which was performed under contract in 2007/08. Andrew Smith is greatly thanked for collecting the EXAFS data at Diamond Light Source.

Appendix A. Supplementary data

Supplementary data to this article can be found online at http://dx.doi.org/10.1016/j.ssi.2012.04.027.

References

[1] X.D. Xiang, X. Sun, G. Brice, Y. Lou, K.A. Wang, H. Chang, W.G. Wallace-Freedman, S.W. Chen, P.G. Schultz, Science 268 (1995) 1738–1740.
[2] X.D. Sun, C. Gao, J. Wang, X.D. Xiang, Appl. Phys. Lett. 70 (1997) 3353–3355.
[3] K. Fujimoto, K. Takada, T. Sasaki, M. Watanabe, Appl. Surf. Sci. 223 (2004) 49–53.
[4] I. Yanase, T. Ohtaki, M. Watanabe, Solid State Ionics 151 (2002) 189–196.
[5] K. Fujimoto, M. Watanabe, Meas. Sci. Technol. 16 (2005) 41–45.
[6] I. Yanase, T. Ohtaki, M. Watanabe, Appl. Surf. Sci. 189 (2002) 292–299.
[7] K. Yajima, Y. Ueda, H. Tsuruya, T. Kanougi, Y. Oumi, S.S.C. Ammal, S. Takami, M. Kubo, A. Miyamoto, Appl. Catal. A-Gen 194 (2000) 183–191.
[8] L. Chen, Y. Zhang, S. Yang, J.R.G. Evans, Rev. Sci. Instrum. 78 (2007) 072210-1–072210-6.
[9] R.C. Pullar, Y. Zhang, L. Chen, S. Yang, J.R.G. Evans, N.M. Alford, J. Eur. Ceram. Soc. 27 (2007) 3861–3865.
[10] R.C. Pullar, Y. Zhang, L. Chen, S. Yang, J.R.G. Evans, P.K. Petrov, A.N. Salak, D.A. Kiselev, A.L. Kholkin, V.M. Ferreira, N. Alford, J. Eur. Ceram. Soc. 27 (2007) 4437–4443.
[11] M. Woodhouse, G. Herman, B. Parkinson, Chem. Mater. 17 (2005) 4318–4324.
[12] J. Choi, H. Park, M. Hoffmann, J. Mater. Res. 25 (2010) 149–158.
[13] Z. Luo, B. Geng, J. Bao, C. Gao, J. Comb. Chem. 7 (2005) 942–946.
[14] M. Kahn, A. Seubsai, I. Onal, S. Senken, Comb. Chem. High Throughput Screen 13 (2010) 67–74.
[15] J. Klein, C. Lehmann, H. Schmidt, W. Maier, Angew. Chem. Int. Ed. 37 (1998) 3369–3372.
[16] J. Thorne, R. Sanderson, J. Dahn, R. Dunlap, J. Electrochem. Soc. 157 (2010) A1085–A1091.
[17] A. Cabanas, J.A. Darr, E. Lester, M. Poliakoff, Chem. Commun. 11 (2000) 901–902.
[18] A.A. Chaudhry, S. Haque, S. Kellici, P. Boldrin, I. Rehman, F.A. Khalid, J.A. Darr, Chem. Commun. (2006) 2286–2288.
[19] A.A. Chaudhry, J. Goodall, M. Vickers, J.K. Cockcroft, I. Rehman, J.C. Knowles, J.A. Darr, J. Mater. Chem. 18 (2008) 5900–5908.
[20] Z. Zhang, S. Brown, J. Goodall, X. Weng, K. Thompson, K. Gong, S. Kellici, R. Clark, J.R.G. Evans, J.A. Darr, J. Alloys Compd. 476 (2009) 451–456.
[21] X. Weng, D. Brett, V. Yufit, P. Shearing, N. Brandon, M. Reece, H. Yan, C. Tighe, J.A. Darr, Solid State Ionics 181 (2010) 827–834.
[22] P. Boldrin, A. Hebb, A. Chaudhry, L. Otley, B. Thiebaut, P. Bishop, J.A. Darr, Ind. Eng. Chem. Res. 46 (2007) 4830–4838.
[23] T. Adschiri, K. Kanazawa, K. Arai, J. Am. Ceram. Soc. 75 (1992) 1019–1022.
[24] X. Weng, J. Cockcroft, G. Hyett, M. Vickers, P. Boldrin, C.C. Tang, S. Thompson, J.E. Parker, J.C. Knowles, I. Rehman, J.R.G. Evans, J.A. Darr, J. Comb. Chem. 11 (2009) 829–834.
[25] T. Lin, S. Kellici, K. Gong, K. Thompson, J.R.G. Evans, X. Wang, J.A. Darr, J. Comb. Chem. 12 (2010) 383–392.
[26] A.J. Dent, G. Cibin, S. Ramos, A.D. Smith, S.M. Scott, L. Varandas, M.R. Pearson, N.A. Krumpa, C.P. Jones, P.E. Robbins, J. Phys. Conf. Ser. 190 (2009) 012039.
[27] L. Van der Pauw, Philips Res. Rep. 13 (1958) 1–9.
[28] E.V. Tsipis, M.V. Patrakeev, J.C. Waerenborgh, Y.V. Pivak, A.A. Markov, P. Gaczynski, E.N. Naumovich, V.V. Kharton, J. Solid State Chem. 180 (2007) 1902–1910.
[29] M. Carvalho, A. Wattiaux, L. Ferreira, J. Bassat, J. Solid State Chem. 182 (2009) 60–64.
[30] G. Amow, J. Au, I. Davidson, Solid State Ionics 177 (2006) 25–1837.
[31] M. Greenblatt, Curr. Opin. Solid State Mater. Sci. 2 (1997) 174–183.
[32] E. Kiselev, N. Proskurnina, V. Voronin, Inorg. Mater. 43 (2007) 167–175.
[33] C. Ling, D. Argyriou, J. Solid State Chem. 152 (1999) 517–525.
[34] Z. Zhang, M. Greenblatt, J. Solid State Chem. 117 (1995) 236–246.
[35] V.I. Voronin, I.F. Berger, V.A. Cherepanov, L.Ya. Gavrilova, A.N. Petrov, A.I. Ancharov, B.P. Tolochko, S.G. Nikitenko, Nucl. Instrum. Methods Phys. Res., Sect. A 470 (2001) 202–209.
[36] G. Amow, I. Davidson, S.J. Skinner, Solid State Ionics 177 (2006) 1205–1210.
[37] H. Beltrán, M. Prades, N. Masó, E. Cordoncillo, A. West, J. Am. Ceram. Soc. 93 (2010) 500–505.
[38] N. Masó, M. Prades, H. Beltrán, E. Cordoncillo, D. Sinclair, A. West, Appl. Phys. Lett. 97 (2010) 062907.